On the definition and analysis of the width of the marginal ice zone

Courtenay Strong*

Department of Atmospheric Science, University of Utah

Dallas Foster

Department of Mathematics, University of Utah

Elena Cherkaev

Department of Mathematics, University of Utah

Ian Eisenman

Scripps Institution of Oceanography

Kenneth M. Golden

Department of Mathematics, University of Utah

Corresponding author address: Courtenay Strong, Department of Atmospheric Sciences, University of Utah, Salt Lake City, Utah, USA.

E-mail: court.strong@utah.edu

ABSTRACT

During the warm season, Arctic sea ice retreats to a central mass of nearly solid ice ("pack ice") surrounded by a band of broken ice called the marginal ice zone (MIZ), which in turn is surrounded by open ocean. The width of the MIZ (distance across the broken ice from pack ice edge to open ocean) is a fundamental length scale for polar physical and biological dynamics. A dramatic 39% widening of the warm-season MIZ since 1979 was recently uncovered by defining MIZ width as the arc length of streamlines through a solution to Laplace's equation describing sea ice concentration within the MIZ. Properties of this definition and analysis method are explored in more detail here. Considering an eccentric annulus as a simplified model of the MIZ geometry, we present eight different definitions of average MIZ width, including variations on the previously used Laplace-based formulation and simpler equations using only area and perimeter. Variations in annulus eccentricity and edge waviness can increase, decrease, or leave unchanged the average width of the annulus depending on how the average is defined. We then apply the eight definitions to MIZ satellite data and find that the average width for any one year varies by as much as 30% depending on how it is defined, but the previously reported widening trend for the warm-season MIZ from 1979-2012 is robust across definitions. Updating the MIZ width results to include 2013 and 2014, we find a dramatic narrowing during the most recent two years of the satellite record, signaling a possible end of the widening trend.

1. Introduction

Declines in Arctic sea ice over the past few decades have been dramatic and appear to be accelerating, particularly during the warm-season (Polyakov et al. 2012; Comiso 2012; Stammerjohn et al. 2012; Cavalieri and Parkinson 2012, and references therein). Record breaking extent minima and abrupt changes in Arctic sea ice properties such as seasonal variability have been observed (Livina and Lenton 2013). These changes in Arctic sea ice suggest scientifically important changes in the position, width, and area of the marginal ice zone (MIZ) – a dynamic and biologically active region that transitions from dense pack ice to open ocean (e.g., Squire 1998; Wadhams 2000; Squire 2007). The width of the MIZ in particular is recognized as a fundamental length scale for climate dynamics and polar ecosystem dynamics (e.g., Wadhams 2000). The MIZ provides a buffer that protects the stable morphology of the inner ice from wave penetration (e.g., Squire 2007) and represents a region over which turbulent atmospheric boundary layer on-ice flows transform into their stable polar form (e.g., Shaw et al. 1991; Glendening 1994). The scale of the MIZ establishes an important spatial dimension for marine habitat selection (e.g., Ribic et al. 1991; Perrette et al. 2010; Post et al. 2013), and impacts human accessibility to the Arctic (Stephenson et al. 2011; Rogers et al. 2012; Schmale et al. 2013; Rogers et al. 2013).

Strong (2012) introduced an objective and automated method for identifying and measuring the width of the MIZ based on sea ice concentrations. Recent application of the method to satellite data (Strong and Rigor 2013) revealed that the warm-season (July-September) Arctic MIZ widened over the past three decades by 39% while moving poleward. A representative warm-season sea ice configuration from early in the satellite record (Fig. 1a) shows a large region of pack ice (gray shading) surrounded by a narrow MIZ (white shading). More recently in the satellite era (Fig. 1b),

the pack ice has retreated more rapidly than the marginal ice, leaving a markedly widened MIZ, particularly toward the left of the figure in the East Siberian and Beaufort Seas.

Studies often report manually retrieved satellite-based estimates of MIZ width for specific regions and time periods (e.g., Comiso et al. 1984), but there are challenges associated with objective definition and automated analysis of MIZ width in part because of the non-convex shape of the MIZ (e.g., Fig. 1b). In medical imaging, Jones et al. (2000) introduced a definition of the width of a non-convex region as the arc length of curves ("streamlines") along $\nabla\phi$, where ϕ is the solution of Laplace's equation ($\nabla^2\phi = 0$) in this region. The desirable properties of this definition include a unique width at every point in the volume or area and the ability to define the width of non-convex shapes. Strong (2012) adapted this definition of width to the MIZ as illustrated in Fig. 1c. In this example, the solution to $\nabla^2\phi = 0$ was obtained numerically with MIZ ice concentration boundary conditions $\phi = 0.80$ on the high-concentration edge adjacent to dense pack ice and $\phi = 0.15$ on the low-concentration edge adjacent to open ocean. Strong (2012) defined MIZ width by averaging the arc length of the streamlines with respect to distance along the perimeter of the MIZ, but other definitions are possible (e.g., averaging the arc lengths with respect to area).

Here we examine several reasonable definitions of average MIZ width by applying Laplace's equation to the eccentric annulus, an analytically tractable model of MIZ geometry. Then we revisit the analysis of MIZ width trends over the satellite era to evaluate sensitivity of the results to the definition of average width. Section 2 introduces the eccentric annulus model, and establishes notation and formulae related to Laplace's equation and width. Three families of average width definitions are presented in Section 3, and effects of changes to width definition at various levels of eccentricity, inner radius, and edge waviness are explored in Sections 4-6. To evaluate width definition effects in MIZ observation data, analysis of MIZ width in satellite-based sea ice concen-

trations is extended in Section 7 to include all the families of definitions. Summary and discussion are provided in Section 8.

2. Eccentric annulus model and Laplace's equation

The geometry of the marginal ice zone (e.g., Fig. 1a,b) can be approximated by an eccentric annulus model (e.g., Figs. 1d,e respectively). In the eccentric annulus model, the MIZ is the annulus (white shading, Figs. 1d,e) defined by a unit radius outer circle at the MIZ-ocean interface and an inner circle at the pack ice-MIZ interface. The eccentric annulus enables us to write analytical solutions for Laplace's equation (e.g., shading in Fig. 1f) and to derive an explicit formula for the arc length of the streamlines (i.e., width) through $\nabla\phi$ (black curves, Fig. 1f) as presented at the end of this section.

Consider Laplace's equation $\nabla^2\phi = 0$ in the eccentric annulus model with geometry shown in Fig. 2a. The function ϕ represents an idealized (smooth) sea ice concentration field within the MIZ modeled by the annulus with boundary conditions $\phi = 0.15$ on the outer edge (marginal ice / ocean interface) and $\phi = 0.80$ on the inner edge (marginal ice / pack ice interface). The outer edge of the marginal ice has radius $r_2 = 1$, the inner edge has radius r_1, and displacement of the pack ice center (x_0) from the origin defines the eccentricity h. Assume that the xy-plane in Fig. 2a represents a complex $z-$plane with $z = x + iy$. Using a conformal mapping detailed in Appendix A, Laplace's equation has a solution given by the complex potential

$$F(z) = \alpha \ln\left(\frac{z-a}{az-1}\right) + k, \tag{1}$$

where a is determined by the geometry of the annulus (x_1 and x_2, Fig. 2a; equation A2), and the constants $k = 0.15$ and $\alpha = (0.80-0.15)/\ln R_0$ are determined by the boundary conditions (R_0 is

given by A3). The real part of $F(z)$ is the potential (Fig. 2b) given by

$$\phi = \alpha \ln \left| \frac{z-a}{az-1} \right| + k, \tag{2}$$

and the imaginary part of $F(z)$ is the stream function (Fig. 2c) given by

$$\psi = \alpha \arg \left(\frac{z-a}{az-1} \right). \tag{3}$$

The solution ϕ represents an idealized sea ice concentration field for the MIZ that transitions smoothly between its boundary conditions (sea ice concentrations 0.80 on the pack ice edge and 0.15 on the ocean edge; e.g., Fig. 1c).

At a point in the annulus Ω, the width ℓ is defined as the arc length of the level set of ψ through that point (example streamline curves representing the level sets of ψ are shown by black contours in Figs. 1c,f and 2c). For the eccentric annulus model, we have an explicit expression for ℓ as a function of ψ

$$\ell(\psi_c/\alpha, a) = \begin{cases} \dfrac{a^2-1}{a\sin(\psi_c/\alpha)} \tan^{-1}\left(\dfrac{at - \cos(\psi_c/\alpha)}{\sin(\psi_c/\alpha)} \right) \Bigg|_{t=1}^{t=R_0}, & \text{if } \psi_c \alpha^{-1} \notin \{0, \pi\}, \\ 1 + x_2, & \text{if } \psi_c \alpha^{-1} = 0, \\ 1 - x_1, & \text{if } \psi_c \alpha^{-1} = \pi, \end{cases} \tag{4}$$

and shading in Fig. 2d shows calculations of width for our eccentric annulus example.

3. Definitions of MIZ average width

In this section, we present eight different definitions for MIZ average width, organized into three subgroups based on common characteristics. Each subgroup provides potentially useful perspectives on the evolving configuration of the MIZ.

a. Width averaged with respect to area

The Laplace method defines width at every point on the eccentric annulus Ω, so one definition of average width to consider is an average with respect to area

$$\bar{\ell}_{\text{area}} = \frac{1}{A_\Omega} \int_\Omega \ell(x,y)\, \mathrm{d}A, \tag{5}$$

where A_Ω is the total area of the annulus and ℓ is defined in equation (4). This is analogous to the averages with respect to volume presented in application of the Laplace solution to width or thickness in medical imaging (Jones et al. 2000). For the annulus, we approximate (5) by evaluating the explicit width formula (4) on a regular grid with uniform spacing in x and y, and then averaging the values.

b. Width averaged with respect to distance along a curve

Here we introduce a different definition of an average width generalizing a definition in Strong (2012) which uses width averaged along the inner and outer perimeters. To establish notation, width averaged with respect to arc length (s) along the curve γ is

$$\bar{\ell}_\gamma = \frac{1}{L_\gamma} \int_\gamma \ell(s)\, \mathrm{d}s, \tag{6}$$

where L_γ is the arc length of the curve γ. For a first specific case of (6), we define width averaged with respect to arc length around the MIZ's outer perimeter γ_{out}

$$\bar{\ell}_{\text{out}} = \frac{1}{L_{\text{out}}} \int_{\gamma_{\text{out}}} \ell(s)\, \mathrm{d}s, \tag{7}$$

where L_{out} is the arc length of the outer perimeter. When applied to the annulus, $L_{\text{out}} = 2\pi r_2$ for its circular outer perimeter (Fig. 2a). Width averaged with respect to arc length along the MIZ's inner perimeter (curve denoted γ_{in}) is

$$\bar{\ell}_{\text{in}} = \frac{1}{L_{\text{in}}} \int_{\gamma_{\text{in}}} \ell(s)\, \mathrm{d}s, \tag{8}$$

where L_{in} is the arc length of the inner perimeter. When applied to the annulus, $L_{\text{in}} = 2\pi r_1$ for its circular inner perimeter (Fig. 2a).

We also consider the average of the outer- and inner-perimeter results

$$\bar{\ell}_{\text{avg}} = \frac{1}{2}(\bar{\ell}_{\text{out}} + \bar{\ell}_{\text{in}}). \tag{9}$$

The approach taken in (Strong 2012) was to average with respect to arc length along the entire (inner and outer) perimeter, which is equivalently the weighted average of $\bar{\ell}_{\text{out}}$ and $\bar{\ell}_{\text{in}}$, where the weighting is the arc length of each perimeter

$$\bar{\ell}_{\text{per}} = \frac{L_{\text{out}}\bar{\ell}_{\text{out}} + L_{\text{in}}\bar{\ell}_{\text{in}}}{L_{\text{out}} + L_{\text{in}}}. \tag{10}$$

Finally, we consider an average with respect to length of a specific level set $\phi = \phi_*$ on the interior of the annulus (i.e., $0.15 < \phi_* < 0.80$)

$$\bar{\ell}_{\phi_*} = \frac{1}{L_{\phi_*}} \int_{\gamma_{\phi_*}} \ell(s)\, \mathrm{d}s, \tag{11}$$

where L_{ϕ_*} is the arc length of the level set $\phi = \phi_*$. When applied to the annulus, L_{ϕ_*} is the circumference of a circle because the level sets of ϕ are circles (Fig. 2b). The value ϕ_* will be chosen so that $\bar{\ell}_{\phi_*} = r_2 - r_1$ as detailed in Section 4b.

The drawback of inner (outer) perimeter based definition is that both the length $L_{in(out)}$ of the curve $\gamma_{in(out)}$ and the integral along this curve may grow without bound with increasing resolution. Here we assume that the resolution is limited so that the length of the curve $\gamma_{in(out)}$ is bounded.

c. Average width from areas and perimeters alone

In this subsection, we consider two definitions of average width that circumvent solving Laplace's equation, instead using only the annulus area and perimeter lengths of the inner and outer circles. For the MIZ, this is a computationally convenient and conceptually attractive approach because the knowledge of function ℓ is not needed.

To motivate the first area-perimeter based definition of average width, we note that for a simple shape like a rectangle, its width is simply area divided by length. Extending that concept to the present context, the width of the annulus may be introduced as the annulus area divided by the length of some curve inside the annulus. In particular, taking the circumference of a circle of radius $(r_1 + r_2)/2$, with the length which is the average of the lengths of the inner and outer circumferences, $\pi(r_2 + r_1)$, results in the definition of annulus width which is the average width $r_2 - r_1$. Hence, we define the width $\bar{\ell}_{\text{ratio}}$ as:

$$\bar{\ell}_{\text{ratio}} = \frac{A_\Omega}{\pi(r_2 + r_1)}, \tag{12}$$

where A_Ω is the area of the annulus. Key properties of this definition include its relative simplicity of application (circumvention of solving Laplace's equation) and its invariance with respect to eccentricity h. For an observed MIZ area not enclosed by circles, a more general form of (12) is

$$\bar{\ell}_{\text{ratio}} = \frac{A_\Omega}{\bar{L}} \tag{13}$$

where $\bar{L}$ is the average of the MIZ outer-boundary and inner-boundary arc lengths, and A_Ω is the area of the MIZ.

We next define an average width that also yields $r_2 - r_1$ for the annulus, but requires only area measurements (i.e., no perimeter). To simplify notation in later sections, we introduce an "effective radius" $\tilde{r}$ which is the radius of a circle of the same area. We define two specific cases of effective radius:

$$\tilde{r}_T = (A_T/\pi)^{1/2} \tag{14a}$$

$$\tilde{r}_P = (A_P/\pi)^{1/2} \tag{14b}$$

where A_P is the pack ice area (analogous to area of inner circle on annulus) and $A_T = A_P + A_\Omega$ is the total ice area (analogous to area within outer circle on annulus). Using this notation, we define

$$\bar{\ell}_{\text{radii}} = \tilde{r}_T - \tilde{r}_P, \tag{15}$$

which yields results that are invariant with respect to eccentricity and also invariant with respect to area-conserving waviness along the edge of the MIZ (explored below in Section 6). Note that (15) is equivalent to (12) when both are applied to an annulus, but (13) and (15) will in general produce different results when applied to a MIZ or an annulus with waviness introduced along its perimeter.

4. Effect of changes to eccentricity

In this section, we examine how the results from the various definitions of annulus average width are affected by changes to eccentricity. Depending on application, sensitivity (or insensitivity) of average width to eccentricity might be a desirable feature. Our baseline case is the concentric annulus (Fig. 3a) whose average width ($\bar{\ell} = r_2 - r_1 = 0.3$) is consistent across all eight definitions in Section 3 (Table 1a-h, column 3a). In the subsections below, we increase the eccentricity from $h = 0$ to $h = 0.25$ (Fig. 3b), and discuss average width based on the various definitions presented in Section 3.

a. Effect of eccentricity on width averaged with respect to area

Width averaged with respect to area ($\bar{\ell}_{\text{area}}$, equation 5) is extremely sensitive to eccentricity because, as the inner circle shifts off center, the portions of the annulus that are becoming wider are also occupying larger area (compare Figs. 3a,b , where $\bar{\ell}_{\text{area}} = 0.300$ for Fig. 3a, while $\bar{\ell}_{\text{area}} = 0.405$ for Fig. 3b). Numerical results for a particular choice of parameters of the annulus, demonstrating the dependence of $\bar{\ell}_{\text{area}}$ on eccentricity are shown in (Table 1a). This rapid increase of $\bar{\ell}_{\text{area}}$ with

eccentricity is shown in Fig. 4a, where the endpoints of the $\bar{\ell}_{\text{area}}$ curve correspond to the change from Fig. 3a (eccentricity $h = 0$) to Fig. 3b (eccentricity $h = 0.25$).

b. Effect of eccentricity on width averaged with respect to distance along a curve

$\bar{\ell}_{\text{out}}$ and $\bar{\ell}_{\text{in}}$ respond oppositely to changes in eccentricity (Fig. 4a). The eccentricity increase from $h = 0$ to $h = 0.25$ (see Fig. 3a and Fig. 3b) resulted in a 6% increase in $\bar{\ell}_{\text{out}}$ (from 0.300 to 0.317; Table 1b) and a 7% decrease in $\bar{\ell}_{\text{in}}$ (from 0.300 to 0.280; Table 1c). To illustrate why $\bar{\ell}_{\text{out}}$ and $\bar{\ell}_{\text{in}}$ respond oppositely to eccentricity, Fig. 5a shows ℓ as a function of angle $\beta \in [0, 2\pi)$ around the annulus's outer circle [denoted $\ell_{\text{out}}(\beta)$] and inner circle [denoted $\ell_{\text{in}}(\beta)$]. The functions $\ell_{\text{out}}(\beta)$ and $\ell_{\text{in}}(\beta)$ have the same range, intersecting at their maximum value [$\ell(\pi) = r_2 - r_1 + h$] and minimum value [$\ell(0) = \ell(2\pi) = r_2 - r_1 - h$], and we observe that $\ell_{\text{out}} \geq \ell_{\text{in}}$ for $\beta \in [0, 2\pi)$. Cosine-like functions $\ell_{\text{out}}(\beta)$ and $\ell_{\text{in}}(\beta)$ resemble a shifted cosine function $\ell_{\cos}(\beta)$:

$$\ell_{\cos}(\beta) = (r_2 - r_1) - h\cos(\beta) \tag{16}$$

that has average $r_2 - r_1$ (Fig. 5a). Fig. 5b shows how ℓ_{out} and ℓ_{in} differ from $\ell_{\cos}$, illustrating that $\ell_{\text{out}} \geq \ell_{\cos}$ and $\ell_{\text{in}} \leq \ell_{\cos}$ for $\beta \in [0, 2\pi)$.

The average of width results from the outer and inner perimeter ($\bar{\ell}_{\text{avg}} = (\bar{\ell}_{\text{out}} + \bar{\ell}_{\text{in}})/2$) is nearly invariant with respect to eccentricity (Fig. 4a), but does decrease slightly with eccentricity because $\bar{\ell}_{\text{in}}$ decreases faster than $\bar{\ell}_{\text{out}}$ increases ($\bar{\ell}_{\text{avg}}$ is 0.300 and 0.299 for Figs. 3a,b, respectively; Table 1d). This result encourages us to seek a width averaged with respect to arc length that is invariant with respect to eccentricity, meaning the average width takes the value $r_2 - r_1$ over the full range of h. One approach, following (Strong 2012), is to average with respect to the total arc length along the inner and outer perimeters, which is equivalently the weighted average of $\bar{\ell}_{\text{out}}$ and $\bar{\ell}_{\text{in}}$, where the weighting is the arc length of each perimeter. For the special case of the annulus, equation (10)

becomes

$$\bar{\ell}_{\text{per}} = \frac{r_2\bar{\ell}_{\text{out}} + r_1\bar{\ell}_{\text{in}}}{r_2 + r_1} \tag{17}$$

because the perimeters are circles (Fig. 2a). $\bar{\ell}_{\text{per}}$ increases slightly with eccentricity (Fig. 4a) because the weight on $\bar{\ell}_{\text{out}}$ is larger than the weight on $\bar{\ell}_{\text{in}}$ by a factor of r_2/r_1, and $\bar{\ell}_{\text{per}}$ has values 0.300 and 0.302 for Figs. 3a,b, respectively (Table 1e).

Probing further for a definition of average width that is invariant with respect to eccentricity, we consider averages with respect to distance along level sets of ϕ on the interior of the annulus (equation 11). The width averaged with respect to distance along circular level sets of ϕ is continuous and monotonic over the range $0.15 \leq \phi \leq 0.80$ (Appendix B). Hence, there exists a unique level set of ϕ (denoted ϕ_*) along which we can average $\ell(\beta)$ to yield the width $r_2 - r_1$ for given radii and eccentricity $\{r_1, r_2, h\}$. To find ϕ_*, we use simplex search method (Lagarias et al. 1998) to minimize $|\bar{\ell} - (r_2 - r_1)|$, and we use $\bar{\ell}_{\phi_*}$ to denote the average width along the level set $\phi = \phi_*$. For the example in Fig. 3b we have $\{r_1 = 1, r_2 = 0.7, h = 0.25, \phi_* = 0.43\}$ and $\bar{\ell}_{\phi_*} = 0.300$ at $h \in \{0, 0.25\}$ (Table 1f). From visual inspection, $\bar{\ell}_{\phi_*}$ appears invariant with respect to h (Fig. 4a), yet it has order 10^{-6} departures from $r_2 - r_1$ over the range $0 < h < 0.25$ (Fig. B1) – a discrepancy too large to attribute to numerical error. More importantly, ϕ_* depends strongly on the radii themselves. For example, Fig. 3c differs from Fig. 3b by a halving of r_1, resulting in a reduction of ϕ_* from 0.43 to 0.30. There is thus not a single ϕ_* that is applicable to all ice configurations, even in the eccentric annulus case, so it is unclear how the ϕ_* concept could be applied to satellite data without arbitrariness.

c. Effect of eccentricity on average width from areas and perimeters

Average width as area-perimeter ratio ($\bar{\ell}_{\text{ratio}}$, equation 12) is unchanged by eccentricity because it is based only on annulus area and perimeter. For Figs. 3a and 3b, $\bar{\ell}_{\text{ratio}} = 0.300$ (Table 1g).

Likewise, the difference between effective radii ($\bar{\ell}_{\text{radii}}$; equation 15) is unchanged by eccentricity because it is based on area alone and is equivalent to $\bar{\ell}_{\text{ratio}}$ for the annulus.

Summarizing variations of average width in response to change in eccentricity $h > 0$ (i.e., change from $h = 0$ to $h = 0.25$, see Fig. 3a, 3b), Table 1 shows

$$\bar{\ell}_{\text{in}} < \bar{\ell}_{\text{avg}} < r_2 - r_1 = \bar{\ell}_{\text{ratio}} = \bar{\ell}_{\text{radii}} = \bar{\ell}_{\phi_*} < \bar{\ell}_{\text{per}} < \bar{\ell}_{\text{out}} < \bar{\ell}_{\text{area}}. \tag{18}$$

5. Effect of changes to inner-outer radii ratio

Here we examine how results from various definitions of annulus average width are affected by changes to inner radius length relative to the outer radius length. A smaller inner radius will of course result in a larger average width for any reasonable definition. With zero eccentricity, all definitions yield $\bar{\ell} = r_2 - r_1$ (Table 1a-h, column 3a), providing a linear and consistent response to changes in r_1. Eccentricity $h > 0$ alters this consistent result across definitions. To illustrate, the annuli in Fig. 3b,c have the same non-zero eccentricity ($h = 0.25$) and the inner radius in Fig. 3c has been halved to $r_1 = 0.35$. All eight definitions explored here yield a larger average width for Fig. 3c than 3b (Table 1a-h, compare columns 3b and 3c), but the values in column 3c vary (i.e., exhibit definition dependence). The dependence of average width on inner radius is approximately linear except for $\bar{\ell}_{\text{area}}$ (Fig. 4b). The reduction in the inner radius from Fig. 3b to 3c did not alter the ranking of the average width results, meaning (18) remained valid.

6. Effect of changes to perimeter waviness

In satellite data, the inner and outer edges of the observed MIZ depart significantly from circularity (e.g., Fig 1a,b). Here we examine how the results from various definitions of annulus average width are affected by changes to perimeter waviness. To begin, we perturb the outer perimeter in

Fig. 3a to

$$r_2 = 1 + \delta \cos(f\beta) \tag{19}$$

where β is angle, $\delta = 0.1$ is the amplitude of the perturbation, and $f = 10$ is the frequency of the perturbation (Fig. 3d). These values for δ and f are chosen to capture scales of variation salient in observed examples (compare Figs. 1a,b and 3d,e). The introduction of this waviness caused the area to increase by $\pi\delta^2/2$, which is approximately 1%. The introduction of this waviness resulted in width decreases along the majority of the inner perimeter (blue shading, Fig. 3d) and a 9% decrease in $\bar{\ell}_{\text{in}}$ to 0.272 (Table 1c; compare columns 3a and 3d). Absolute changes in $\bar{\ell}_{\text{area}}$, $\bar{\ell}_{\text{out}}$, $\bar{\ell}_{\text{avg}}$, and $\bar{\ell}_{\text{per}}$ were no larger than 3% (Table 1a,b,d,e; compare columns 3a and 3d). The very small change in $\bar{\ell}_{\text{area}}$ is especially notable in contrast to its sensitivity to eccentricity highlighted in Section 4a. $\bar{\ell}_{\text{ratio}}$ decreased by 7% as a result of perturbing the outer edge (Table 1g; compare columns 3a and 3d). $\bar{\ell}_{\text{radii}}$ increased by approximately 1% because of the slight increase in annulus area from the waviness (Table 1h; compare columns 3a and 3d).

Next we construct Fig. 3e by perturbing the radius of the inner circle as in (19), but with $f = 7$, chosen so that the wavelength of the perturbation is the same in Figs. 3d,e (i.e., $2\pi/10 = 2\pi 0.7/7$). The introduction of this waviness caused the area to decrease by $\pi\delta^2/2$, which is approximately 1%. The introduction of this waviness produced average width results essentially opposite to waviness on the outer edge. Specifically, widths decreased along the majority of the outer perimeter (blue shading, Fig. 3e) and $\bar{\ell}_{\text{out}}$ decreased by 8% to 0.276 (Table 1c; compare columns 3a,3e). Absolute changes in $\bar{\ell}_{\text{area}}$, $\bar{\ell}_{\text{out}}$, $\bar{\ell}_{\text{avg}}$, and $\bar{\ell}_{\text{per}}$ were no larger than 4% (Table 1a,c,d,e; compare columns 3a and 3e). $\bar{\ell}_{\text{ratio}}$ decreased by 8% because the inner edge lengthened (Table 1g; compare columns 3a and 3e). $\bar{\ell}_{\text{radii}}$ decreased by less than 1% because of the slight decrease in annulus area from the waviness (Table 1h; compare columns 3a and 3e).

The above analysis indicates that lengthening of one edge by waviness tends to modestly increase the average width measured along the wavy edge and more substantially decrease the average width measured along the non-wavy edge for Laplace-based definitions and also ℓ_{ratio}. These changes in average width are further illustrated in Figs. 4c,d where waviness is progressively increased in amplitude from $\delta \in \{0, 0.01, \cdots, 0.1\}$ along the outer and inner edges, respectively. As noted above, we chose the wavelengths in examples in Fig. 3d,e to represent variations salient in observations. Exploring effects over the ranges $0 \leq \delta \leq 0.2$ and $2 \leq f \leq 12$, the decrease in width on the non-wavy edge appears robust, but width measured from the wavy edge can decrease monotonically for more extreme values of f (not shown).

7. Application to satellite data

Here, we use satellite-based sea ice concentration data to analyze how conclusions about MIZ width are sensitive to the definition of average width. The $\bar{\ell}_{\text{per}}$ curve in Fig. 6 extends the analysis of (Strong and Rigor 2013) through near-present, and results from the additional definitions of average width are included for comparison ($\bar{\ell}_{\text{in}}, \bar{\ell}_{\text{avg}}, \bar{\ell}_{\text{ratio}}, \bar{\ell}_{\text{radii}}, \bar{\ell}_{\text{out}}$, and $\bar{\ell}_{\text{area}}$). We do not include $\bar{\ell}_{\phi_*}$ here as this definition requires arbitrariness in how it would be applied to satellite data, as noted in Section 4b. Laplace-based definitions and $\bar{\ell}_{\text{ratio}}$ produced a clustering of similar results with lower average widths, and $\bar{\ell}_{\text{area}}$ and $\bar{\ell}_{\text{radii}}$ produced widths approximately 30% larger than the other definitions. The various definitions yield time series that are positively correlated ($0.791 \leq r \leq 0.998$), each capturing the previously documented MIZ widening from 1979-2012 followed by a dramatic return to narrower MIZ during 2013-2014.

The width $\bar{\ell}_{\text{in}}$ was generally larger than $\bar{\ell}_{\text{out}}$, which is consistent with the tendency for enhanced waviness on the inner edge of the MIZ relative to the outer edge (the inner MIZ perimeter was on average 8% longer than the outer MIZ perimeter). $\bar{\ell}_{\text{avg}}$ was very similar to $\bar{\ell}_{\text{per}}$ as anticipated from

analysis of the eccentric annulus model, and the computationally efficient $\bar{\ell}_{\text{ratio}}$ also yielded a time series very similar to $\bar{\ell}_{\text{per}}$.

Recall from Section 3c the equivalence $\bar{\ell}_{\text{radii}} = \bar{\ell}_{\text{ratio}}$ for the annulus, but for the MIZ we observe in Fig. 6 that $\bar{\ell}_{\text{radii}}/\bar{\ell}_{\text{ratio}} =\approx 1.3$. $\bar{\ell}_{\text{radii}}$ and $\bar{\ell}_{\text{ratio}}$ are both invariant with respect to eccentricity, so the ratio 1.3 largely results from the prominent edge waviness in the observed MIZ (e.g., Fig. 1a,b). To explore this result quantitatively, we write the ratio $\bar{\ell}_{\text{radii}}/\bar{\ell}_{\text{ratio}}$ in terms of effective radii (14a,14b)

$$\frac{\bar{\ell}_{\text{radii}}}{\bar{\ell}_{\text{ratio}}} = \frac{\tilde{r}_T - \tilde{r}_P}{\left(\frac{A_T - A_P}{\bar{L}}\right)} = \frac{\bar{L}}{\pi(\tilde{r}_T + \tilde{r}_P)}, \tag{20}$$

and we see the ratio is unity when the average of the inner and outer MIZ perimeter lengths ($\bar{L}$) is equal to the "effective circumference" $\pi(\tilde{r}_T + \tilde{r}_P)$ introduced in Section 3c. Casting the ice areas as equivalent-area circles minimizes their perimeters per the isoperimetric inequality, so $\pi(\tilde{r}_T + \tilde{r}_P)$ is a lower bound for $\bar{L}$. We find in satellite data that the observed $\bar{L}$ is approximately 1.3 times larger than $\pi(\tilde{r}_T + \tilde{r}_P)$, explaining the ratio $\bar{\ell}_{\text{radii}}/\bar{\ell}_{\text{ratio}} =\approx 1.3$.

Finally, $\bar{\ell}_{\text{area}}$ was also approximately 30% larger than results from most of the other definitions. The similarity in magnitude between $\bar{\ell}_{\text{area}}$ and $\bar{\ell}_{\text{radii}}$ is a coincidence stemming from the particular geometry of the MIZ and does not hold generally across annulus configurations we explored (e.g., Table 1a,h; column 3b). The relative largeness of $\bar{\ell}_{\text{area}}$ stems from the observed MIZ tending to be eccentric (e.g., Fig. 1b) and for its wider portions tending to have larger areas (effect explored in Section 4a).

The widening of the MIZ stemmed from pack ice decline outpacing total ice decline. Recalling the definition of $\bar{\ell}_{\text{radii}}$ from equation (15), it is more precisely relative changes in the equivalent radii of these two areas that are relevant to the width increase, and we see from Fig. 6b that $\tilde{r}_P$ decline outpaced $\tilde{r}_T$ decline with both trending downward (-87 km decade^{-1} for $\tilde{r}_P$ versus -63

km decade^{-1} for $\tilde{r}_T$). The correlation between $\tilde{r}_T$ and $\tilde{r}_P$ is very strong ($r = 0.98$), even after detrending ($r = 0.93$), but $\tilde{r}_P$ is slightly more volatile and accounts for more interannual variance in $\bar{\ell}_{\text{radii}}$ ($r^2 = 0.75$ for $\tilde{r}_P$ versus 0.55 for $\tilde{r}_T$).

8. Summary and discussion

Insight into the effects of eight different definitions of average MIZ width was obtained by considering an eccentric annulus as a simplified model of the MIZ geometry. Introducing variations in eccentricity and edge waviness to the annulus was found to increase, decrease, or leave unchanged the average annulus width depending on how average width is defined. We then applied the eight definitions of average width to MIZ satellite data and found that mean width for any one year varied by as much as 30% depending on how it was defined, but the previously reported widening trend for the warm-season MIZ from 1979-2012 was robust across definitions, as was the dramatic return to narrower MIZ during the two most recent years of the satellite record (2013-2014).

If the distribution of MIZ widths on a particular day is desired, Laplace-based techniques and definitions provide an objective method, and summary statistics such as mean can also be generated from the distribution of widths. Waviness and eccentricity can cause divergent results for width averaged along the inner edge versus the outer edge, suggesting utility in using an average of the inner-edge and outer-edge widths ($\bar{\ell}_{\text{avg}}$), or a perimeter-weighted average ($\bar{\ell}_{\text{per}}$) as in (Strong 2012). Averaging the Laplace-based results with respect to area ($\bar{\ell}_{\text{area}}$) emphasized wider (larger area) parts of the MIZ, yielding values on average 1.3 times larger than the other Laplace-based methods.

When the distribution of widths around the domain is not required, computationally efficient approaches based on area and perimeter length may provide useful perspectives. A simple ratio of the area to the average of the inner and outer perimeter lengths ($\bar{\ell}_{\text{ratio}}$) yields values very similar to

the more computationally complex Laplace-based methods and is recommended as an accessible approximation. An average width based on areas alone was also considered ($\bar{\ell}_{\text{radii}}$), featuring the potentially desirable properties of invariance with respect to eccentricity and with respect to area-conserving edge waviness. $\bar{\ell}_{\text{radii}}$ entirely smooths out waviness on the MIZ perimeters, casting the total ice and pack ice regions as equivalent-area circles, yielding average widths approximately 1.3 times larger than $\bar{\ell}_{\text{ratio}}$.

Our Laplace-based width definition provides a unique width for every point on the MIZ and can be objectively and consistently applied to long term satellite records without discipline-driven or temporally varying changes to the basic formulation. Specific research questions may motivate selection of a particular definition of average width, or formulation of a new one. For example, width averaged with respect to distance along the inner perimeter of the MIZ may be relevant to study of a polar bear approaching the MIZ to hunt from the pack ice. Conversely, a vessel approaching the MIZ from the open ocean edge may be more interested in width averaged with respect to distance along the outer perimeter of the MIZ. A width could also be defined along the direction of wave propagation for oceanic applications, or along the prevailing wind direction for investigation of atmospheric boundary layer modification.

Acknowledgments. We gratefully acknowledge support from the Division of Mathematical Sciences at the U.S. National Science Foundation (NSF) through grants DMS-1413454 and DMS-0940249. We are also grateful for support from the Arctic and Global Prediction Program at the Office of Naval Research (ONR) through Grant N00014-13-10291. Finally, we would like to thank the NSF Math Climate Research Network (MCRN) for their support of this work.

APPENDIX A

Solution to Laplace's equation

We consider an annulus Ω (shown in white in Fig. 2) on the z-plane. Its outer circle centered at the origin, is scaled to have unit radius $r_2 = 1$. This represents the outer boundary of the MIZ at the marginal ice / ocean interface where sea ice concentration $\phi = 0.15$. Its inner circle with radius r_1, is centered at $x_0 \in (r_1 - 1, 1 - r_1)$, and represents the inner boundary of the MIZ at the marginal ice / pack ice interface where $\phi = 0.80$. Ω is mapped to the area between concentric circles in the w-plane (Fig. A1) via the linear fractional transformation (e.g., Brown and Churchill 2009)

$$w = \frac{z - a}{az - 1} \tag{A1}$$

where a is given by

$$a = \frac{1 + x_1 x_2 + \left[(1 - x_1^2)(1 - x_2^2)\right]^{\frac{1}{2}}}{x_1 + x_2}. \tag{A2}$$

The inner circle on the z-plane is mapped to a circle on the w-plane with center at the origin and radius

$$R_0 = \frac{1 - x_1 x_2 + \left[(1 - x_1^2)(1 - x_2^2)\right]^{\frac{1}{2}}}{x_1 - x_2}. \tag{A3}$$

On the w-plane, Laplace's equation $\nabla^2 \Phi = 0$ has solution given by the complex potential

$$F(w) = \alpha \ln w + k. \tag{A4}$$

which has real part $\phi = \alpha \ln |w| + k$ called the potential and imaginary part $\psi = \alpha \arg w$ called the stream function. Boundary conditions $\phi(|w| = R_0) = 0.80$ and $\phi(|w| = 1) = 0.15$ yield $k = 0.15$ and $\alpha = (0.80 - 0.15)/\ln R_0$. Functions ϕ and ψ on the z-plane are respectively given by

$$\phi = \alpha \ln \left| \frac{z - a}{az - 1} \right| + k \tag{A5}$$

$$\psi = \alpha \arg \left(\frac{z - a}{az - 1} \right). \tag{A6}$$

The width ℓ of the annulus Ω at any point can be defined as the arc length of the level set of ψ through that point on the z-plane. On the w-plane, the level set $\{w \in \mathbb{C} : \psi = \psi_c\}$ is the parametric line

$$w(t) = te^{i\psi_c/\alpha};\ \ 1 \le t \le R_0, \tag{A7}$$

which is mapped to the z-plane as

$$z(t) = \frac{te^{i\psi_c/\alpha} - a}{ate^{i\psi_c/\alpha} - 1};\ \ 1 \le t \le R_0. \tag{A8}$$

The modulus of the derivative in (A8) is given by

$$\left|z'(t)\right| = \frac{a^2 - 1}{a^2t^2 - 2at\cos(\psi_c/\alpha) + 1}, \tag{A9}$$

and so for the arc length

$$\ell := \int_1^{R_0} \left|z'(t)\right| \, \mathrm{d}t \tag{A10}$$

we have equation (4) in the main text.

APPENDIX B

Existence and uniqueness of ϕ_*

We consider function (4) and introduce a variable $\tau = \psi_c/\alpha$ in the same domain. Using the arctangent addition property, we rewrite $\ell(\tau)$ as:

$$\ell(\tau) = \begin{cases} \frac{a^2-1}{a\sin(\tau)} \tan^{-1} \frac{a(R_0-1)\sin(\tau)}{1+a^2R_0-a(1+R_0)\cos(\tau)} & \text{if } \tau \notin \{0, \pi\} \\ 1 + x_2 & \text{if } \tau = 0 \\ 1 - x_1 & \text{if } \tau = \pi \end{cases} \tag{B1}$$

This function will be considered on the restricted domain $\tau \in [0, \pi]$ as the objects studied in this case are symmetric with regard to the top and bottom half of the annular domain. To show that for

a given specific length, the appropriate level set of ψ exists and is unique, we will show that this function is continuous and monotonic, and hence, possesses the intermediate value property.

First, we notice that the function $\ell(\tau)$ in (B1) is continuous on the interval $0 < \tau < \pi$ as a composition of continuous functions. Therefore, the only points where the continuity of $\ell(\tau)$ comes into question is at the endpoints, 0 and π. To check the behavior of the function at these points, we calculate the limits of $\ell(\tau)$ when τ goes to zero and to π using l'Hôpital's rule as both limits are indeterminate. Using expressions for a and R_0 (A2 - A3) and with some algebra we obtain:

$$\lim_{\tau\to 0^+} \ell(\tau) = \frac{(a+1)(R_0-1)}{aR_0-1} = 1+x_2$$
$$\lim_{\tau\to \pi^-} \ell(\tau) = \frac{(a-1)(R_0-1)}{aR_0+1} = 1-x_1$$

Since the limits match the definition of $\ell(\tau)$ in (B1), we conclude that this function is continuous.

Now we show that the function $\ell(\tau)$ in (B1) is monotonic. In order to show this, we make some observations. First, note that we are specifically referring to the monotonicity with respect to the variable τ, and only on the domain mentioned earlier. Let us split this domain into two halves. First, consider the behavior of the function on the interval $[0, \pi/2]$. The denominator of $\ell(\tau)$ is increasing whilst the interior of the arctangent is decreasing. These effects combine to produce a net monotonic decrease in the interval. On the second half, from $[\pi/2, \pi]$, the arctangent term tends to zero much faster than the denominator as a result of the combined effects of it's interior composition. One can check that the derivative at $\tau = \frac{\pi}{2}$ is $\frac{-a(a^2-1)(R_0^2-1)}{((1+a^2R_0)^2+a^2(R_0-1)^2)}$. The function exhibits monotonically decreasing behavior as it limits towards $1-x_1$.

From these analytic results, we glean several useful pieces of information. First, since the function (B1) is continuous, it has the intermediate value property. This translates to the fact that every

length between $1+x_2$ to $1-x_1$ exists and has a corresponding value of ψ. The fact that (B1) is monotonic also means that the each unique length has a unique value of ψ. There exists no two stream-functions, ψ, that have the same length on $(0,\pi)$. Finally, since the potential function (2) is harmonic, $\bar{\ell}_{\phi_*}$ inherits both of these properties. Continuity is preserved by the integration, and monotonicity is preserved by the positive nature of the function (B1).

References

Brown, J. W., and R. V. Churchill, 2009: *Complex Variables and Applications*. McGraw-Hill.

Cavalieri, D. J., and C. L. Parkinson, 2012: Arctic sea ice variability and trends, 1979-2010. *The Cryosphere Discussions*, **6 (2)**, 957–979, doi:10.5194/tcd-6-957-2012, URL http://www.the-cryosphere-discuss.net/6/957/2012/.

Comiso, J., S. Ackley, and A. Gordon, 1984: Antarctic sea ice microwave signatures and their correlation with in situ ice observations. *Journal of Geophysical Research: Oceans (1978–2012)*, **89 (C1)**, 662–672.

Comiso, J. C., 2012: Large decadal decline of the Arctic multiyear ice cover. *J. Climate*, **25 (4)**, 1176–1193, doi:10.1175/JCLI-D-11-00113.1, URL http://dx.doi.org/10.1175/JCLI-D-11-00113.1.

Glendening, J. W., 1994: Dependence of boundary layer structure near an ice-edge coastal front upon geostrophic wind direction. *J. Geophys. Res.*, **99 (D3)**, 5569–5581, URL http://dx.doi.org/10.1029/93JD02925.

Jones, S. E., B. R. Buchbinder, and I. Aharon, 2000: Three-dimensional mapping of cortical thickness using Laplace's equation. *Hum. Brain Mapp.*, **11**, 12–32.

Lagarias, J., J. A. Reeds, M. H. Wright, and P. E. Wright, 1998: Convergence properties of the nelder-mead simplex method in low dimensions. *SIAM Journal of Optimization*, **9**, 112–147.

Livina, V. N., and T. M. Lenton, 2013: A recent tipping point in the Arctic sea-ice cover: abrupt and persistent increase in the seasonal cycle since 2007. *The Cryosphere*, **7 (1)**, 275–286, doi: 10.5194/tc-7-275-2013, URL http://www.the-cryosphere.net/7/275/2013/.

Perrette, M., A. Yool, G. D. Quartly, and E. E. Popova, 2010: Near-ubiquity of ice-edge blooms in the Arctic. *Biogeosciences Discuss.*, **7 (6)**, 8123–8142, doi:10.5194/bgd-7-8123-2010.

Polyakov, I. V., J. E. Walsh, and R. Kwok, 2012: Recent Changes of Arctic Multiyear Sea Ice Coverage and the Likely Causes. *Bull. Amer. Meteor. Soc.*, **93 (2)**, 145–151, doi:10.1175/ BAMS-D-11-00070.1, URL http://dx.doi.org/10.1175/BAMS-D-11-00070.1.

Post, E., and Coauthors, 2013: Ecological Consequences of Sea-Ice Decline. *Science*, **341 (6145)**, 519–524, doi:10.1126/science.1235225, URL http://www.sciencemag.org/content/341/6145/ 519.abstract.

Ribic, C. A., D. G. Ainley, and W. Fraser, 1991: Habitat selection by marine mammals in the marginal ice zone. *Antarctic Science, 3 , pp 181-186 doi:10.1017/S0954102091000214*, **3**.

Rogers, T. S., J. E. Walsh, T. S. Rupp, L. W. Brigham, and M. Sfraga, 2012: Future Arctic marine access: analysis and evaluation of observations, models, and projections of sea ice. *The Cryosphere Discussions*, **6 (5)**, 3963–3998, doi:10.5194/tcd-6-3963-2012, URL http: //www.the-cryosphere-discuss.net/6/3963/2012/.

Rogers, T. S., J. E. Walsh, T. S. Rupp, L. W. Brigham, and M. Sfraga, 2013: Future Arctic marine access: analysis and evaluation of observations, models, and projections of sea ice. *The*

Cryosphere, **7 (1)**, 321–332, doi:10.5194/tc-7-321-2013, URL http://www.the-cryosphere.net/7/321/2013/.

Schmale, J., M. Lisowska, and M. Smieszek, 2013: Future Arctic Research: Integrative Approaches to Scientific and Methodological Challenges. *Eos, Transactions American Geophysical Union*, **94 (33)**, 292–292, doi:10.1002/2013EO330004, URL http://dx.doi.org/10.1002/2013EO330004.

Shaw, W. J., R. L. Pauley, T. M. Gobel, and L. F. Radke, 1991: A Case Study of Atmospheric Boundary Layer Mean Structure for Flow Parallel to the Ice Edge: Aircraft Observations From CEAREX. *J. Geophys. Res.*, **96 (C3)**, 4691–4708, URL http://dx.doi.org/10.1029/90JC01953.

Squire, V., 2007: Of ocean waves and sea-ice revisited. *Cold Regions Science and Technology*, **49 (2)**, 110 – 133, doi:10.1016/j.coldregions.2007.04.007, URL http://www.sciencedirect.com/science/article/pii/S0165232X07000870.

Squire, V. A., 1998: The marginal ice zone. *Physics of Ice-covered Seas*, M. Lepparanta, Ed., Vol. 1, Helsinki University Printing House, 381–446.

Stammerjohn, S., R. Massom, D. Rind, and D. Martinson, 2012: Regions of rapid sea ice change: An inter-hemispheric seasonal comparison. *Geophys. Res. Lett.*, **39 (6)**, L06 501–, URL http://dx.doi.org/10.1029/2012GL050874.

Stephenson, S. R., L. C. Smith, and J. A. Agnew, 2011: Divergent long-term trajectories of human access to the Arctic. *Nature Clim. Change*, **1 (3)**, 156–160.

Strong, C., 2012: Atmospheric influence on Arctic marginal ice zone position and width in the Atlantic sector, February-April 1979-2010. *Climate Dynamics*, **39**, 3091–3102, doi:10.1007/s00382-012-1356-6.

476 Strong, C., and I. G. Rigor, 2013: Arctic marginal ice zone trending wider in summer and narrower
477 in winter. *Geophys. Res. Lett.*, **40 (18)**, 4864–4868, URL http://dx.doi.org/10.1002/grl.50928.

478 Wadhams, P., 2000: *Ice in the Ocean*. Gordon and Breach Science Publishers, London, 351 pp.

LIST OF TABLES

TABLE 1. Average annulus width for eight different definitions of average width (a-h). Columns indicate the associated formula, the equation number, and the average width for the examples in Figs. 3a-e.

definition	formula	equation	Fig. 3a	Fig. 3b	Fig. 3c	Fig. 3d	Fig. 3e
a. with respect to area	$\bar{\ell}_{\text{area}} = \frac{1}{A_\Omega}\int_\Omega \ell(x,y)\,\mathrm{d}A$	(5)	0.300	0.405	0.702	0.298	0.293
with respect to distance							
b. along outer perimeter	$\bar{\ell}_{\text{out}} = \frac{1}{L_{\text{out}}}\int_{\gamma_{\text{out}}} \ell(s)\,\mathrm{d}s$	(7)	0.300	0.317	0.670	0.310	0.276
c. along inner perimeter	$\bar{\ell}_{\text{in}} = \frac{1}{L_{\text{in}}}\int_{\gamma_{\text{in}}} \ell(s)\,\mathrm{d}s$	(8)	0.300	0.280	0.623	0.272	0.303
d. average of ℓ_{out} and ℓ_{in}	$\bar{\ell}_{\text{avg}} = \frac{1}{2}(\bar{\ell}_{\text{out}} + \bar{\ell}_{\text{in}})$	(9)	0.300	0.299	0.646	0.291	0.289
e. weighted average of ℓ_{out} and ℓ_{in}	$\bar{\ell}_{\text{per}} = \frac{L_{\text{out}}\bar{\ell}_{\text{out}} + L_{\text{in}}\bar{\ell}_{\text{in}}}{L_{\text{out}} + L_{\text{in}}}$	(10)	0.300	0.302	0.657	0.300	0.300
f. along level set of ϕ	$\bar{\ell}_{\phi^*} = \frac{1}{L_{\phi^*}}\int_{\gamma_{\phi^*}} \ell(s)\,\mathrm{d}s$	(11)	0.300	0.300	0.650	N/A	N/A
from areas and perimeters							
g. area-perimeter ratio	$\bar{\ell}_{\text{ratio}} = A_\Omega/\bar{L}$	(13)	0.300	0.300	0.650	0.280	0.275
h. difference between effective radii	$\bar{\ell}_{\text{radii}} = \tilde{r}_T - \tilde{r}_P$	(15)	0.300	0.300	0.650	0.303	0.298

LIST OF FIGURES

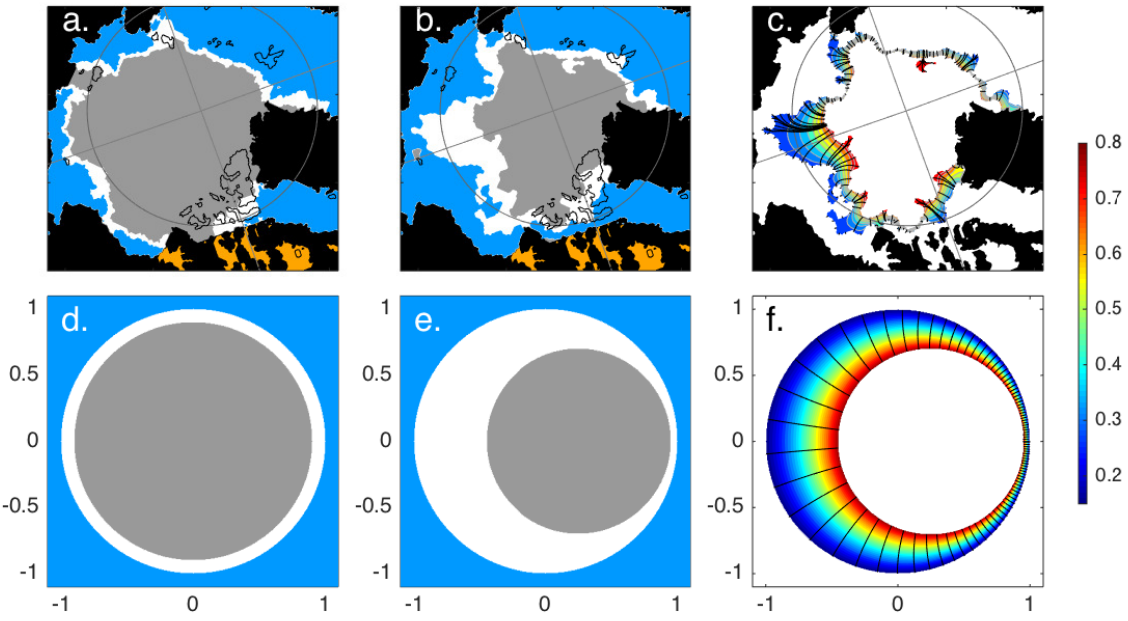

FIG. 1. (a) For 18 September 1984, pack ice is shaded gray, the marginal ice zone is shaded white, and sparse ice and open ocean are shaded blue. Land is shaded black, islands over which concentrations were interpolated are outlined in black, and bays or inland seas where the MIZ was not analyzed are shaded orange. (b) Same as (a), but for 29 August 2010. (c) The solution to Laplace's equation within the MIZ (ϕ) is shaded, and black curves are streamlines through ϕ whose arc length define MIZ width. The lower row shows how eccentric annulus models can be used to approximate the observed patterns in the upper row. Specifically, (d-e) are eccentric annuli (white shading) that approximate the geometry in (a-b), respectively. (f) A simplified, eccentric annulus version of (c) constructed by solving Laplace's equation within the MIZ from (e).

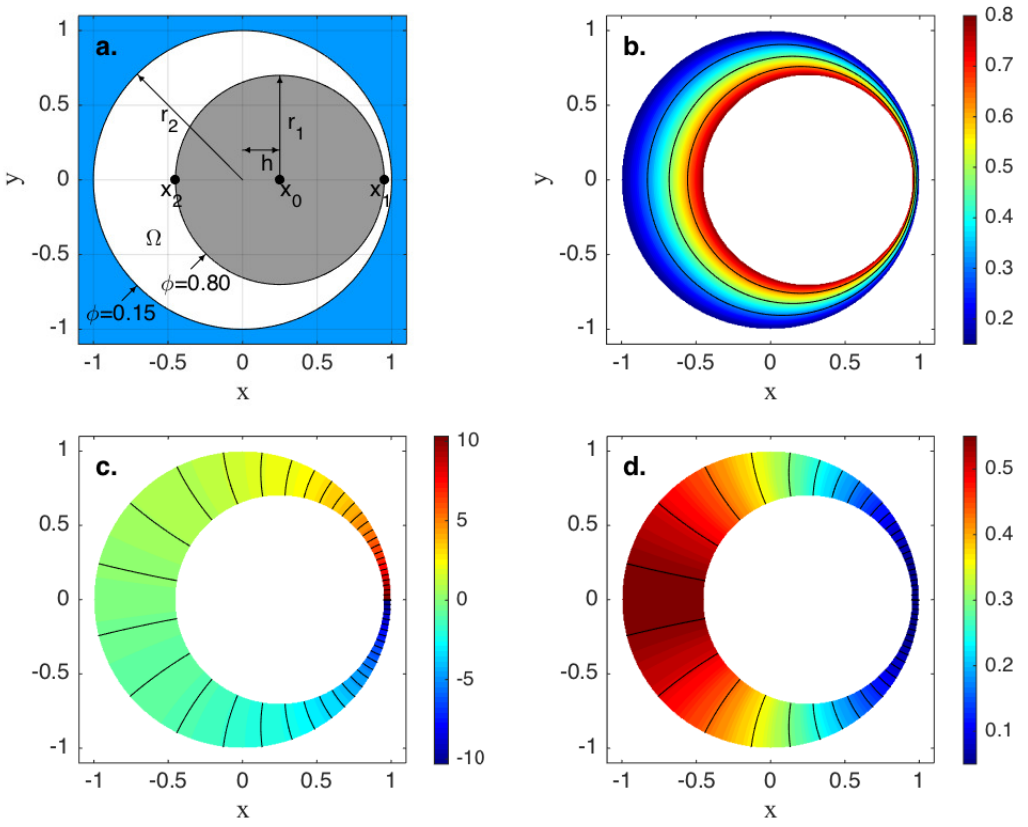

FIG. 2. (a) Schematic indicating notation for the eccentric annulus model: $r_1 = x_1 - x_0$ is radius of inner circle, $r2 = 1$ is radius of outer circle, the inner circle's center x_0 is offset from the origin by eccentricity h, and the annulus is denoted by Ω. (b) The real part of the solution to Laplace's equation within the annulus (ϕ), and (c) the imaginary part (ψ). (d) Shading indicates the width of the annulus (ℓ) at a particular point defined by the arc length of the stream line (level set of ψ) through that point.

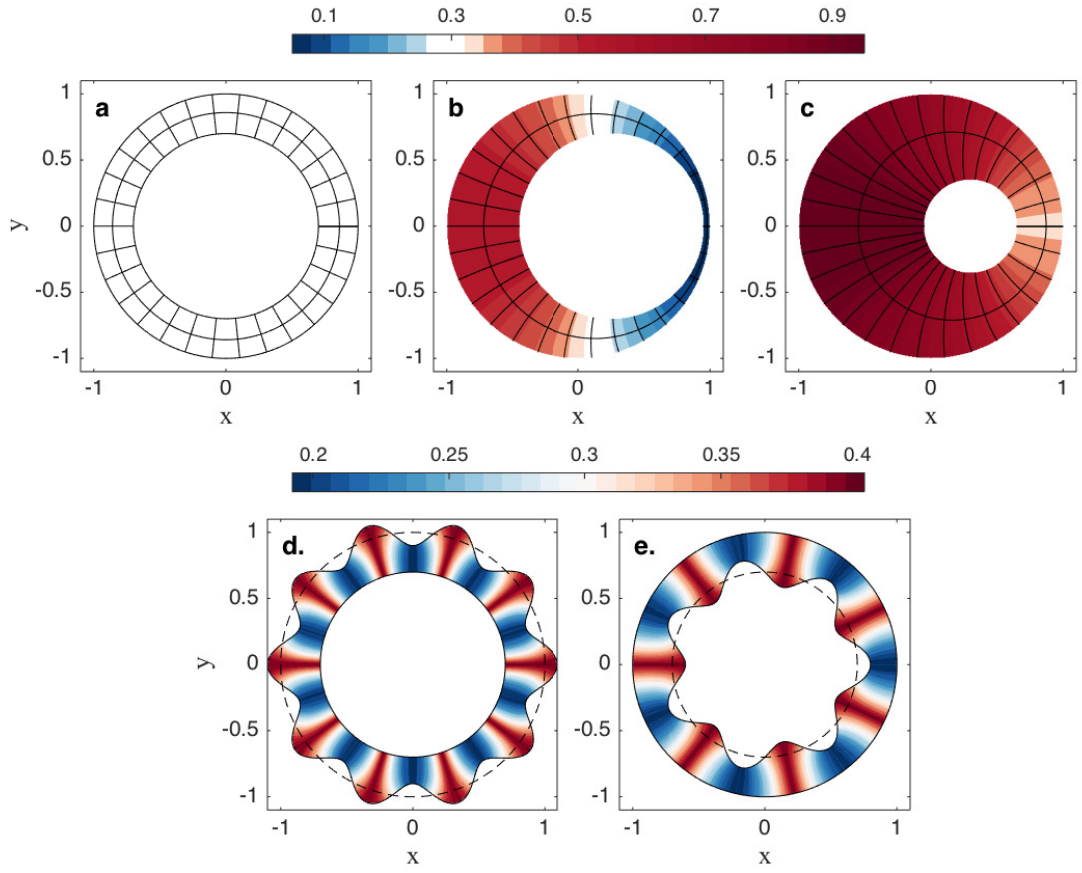

FIG. 3. Shading indicates the width of the annulus (ℓ) at a particular point defined by the arc length of the stream line (level set of ψ) through that point. Each panel is an eccentric annulus example used to illustrate the effect of eccentricity h and inner circle radius r_1: (a) $h = 0, r_1 = 0.7$. (b) $h = 0.25, r_1 = 0.7$. (c) $h = 0.25, r_1 = 0.35$. Examples used to illustrate the effect of (d) waviness on the outer edge with $\{\delta = 0.1, f = 10, \bar{r_1} = 1, r_2 = 0.7, h = 0\}$ (see equation 19), and (e) waviness on the inner edge with $\{\delta = 0.1, f = 7, r_1 = 1, \bar{r_2} = 0.7, h = 0\}$.

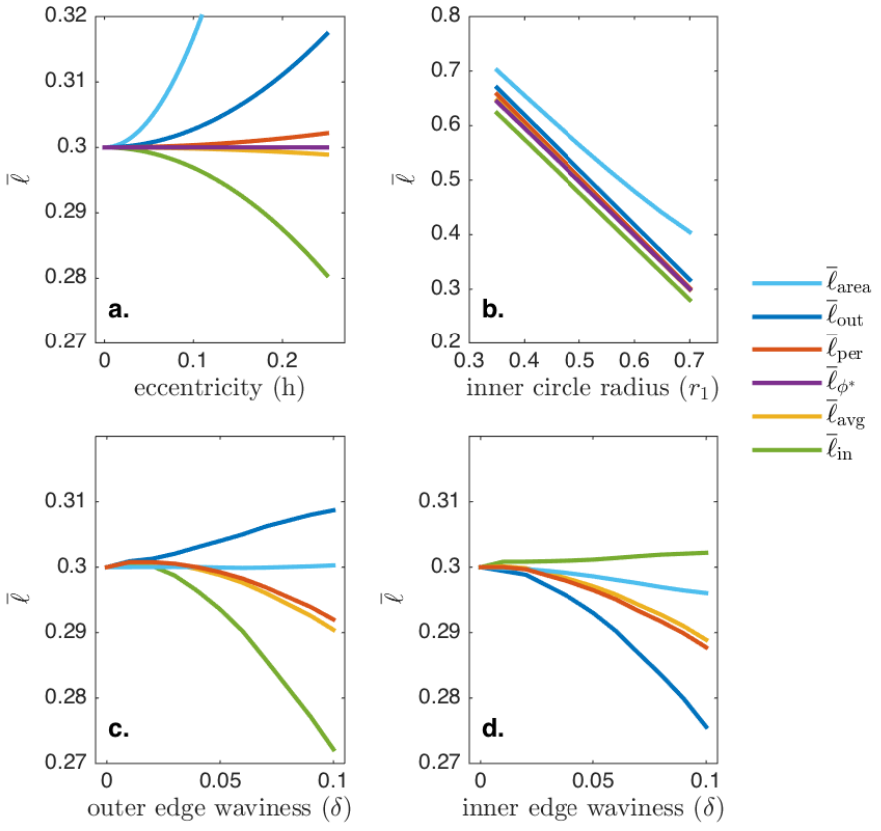

FIG. 4. For various definitions of average MIZ width, dependence on (a) eccentricity, (b) inner circle radius, (c) waviness on the outer edge quantified by δ in equation (19), and (d) waviness on the inner edge quantified by δ in equation (19).

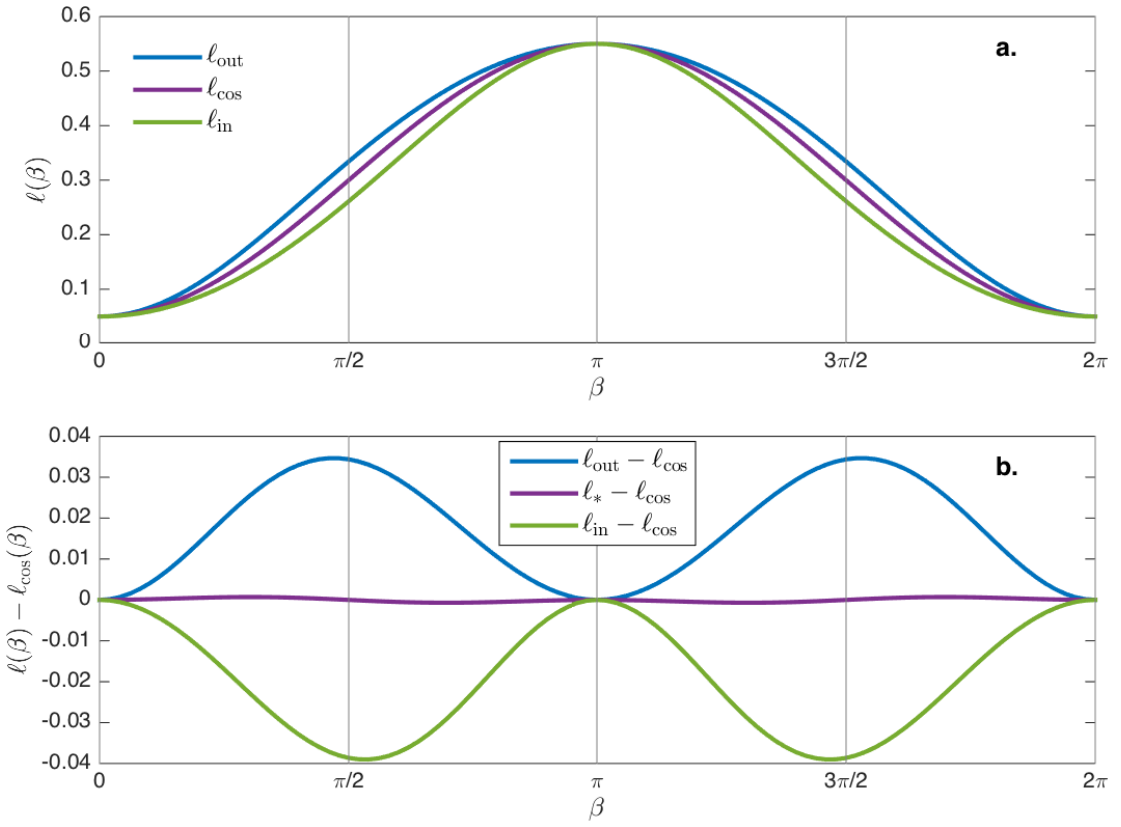

FIG. 5. (a) MIZ width as a function of angle around the annulus's outer circle (ℓ_{out}) and inner circle (ℓ_{in}). ℓ_{cos} is equation (16) shown for reference. (b) Curves show how ℓ_{out}, ℓ_{in}, and ℓ_* differ from ℓ_{cos}.

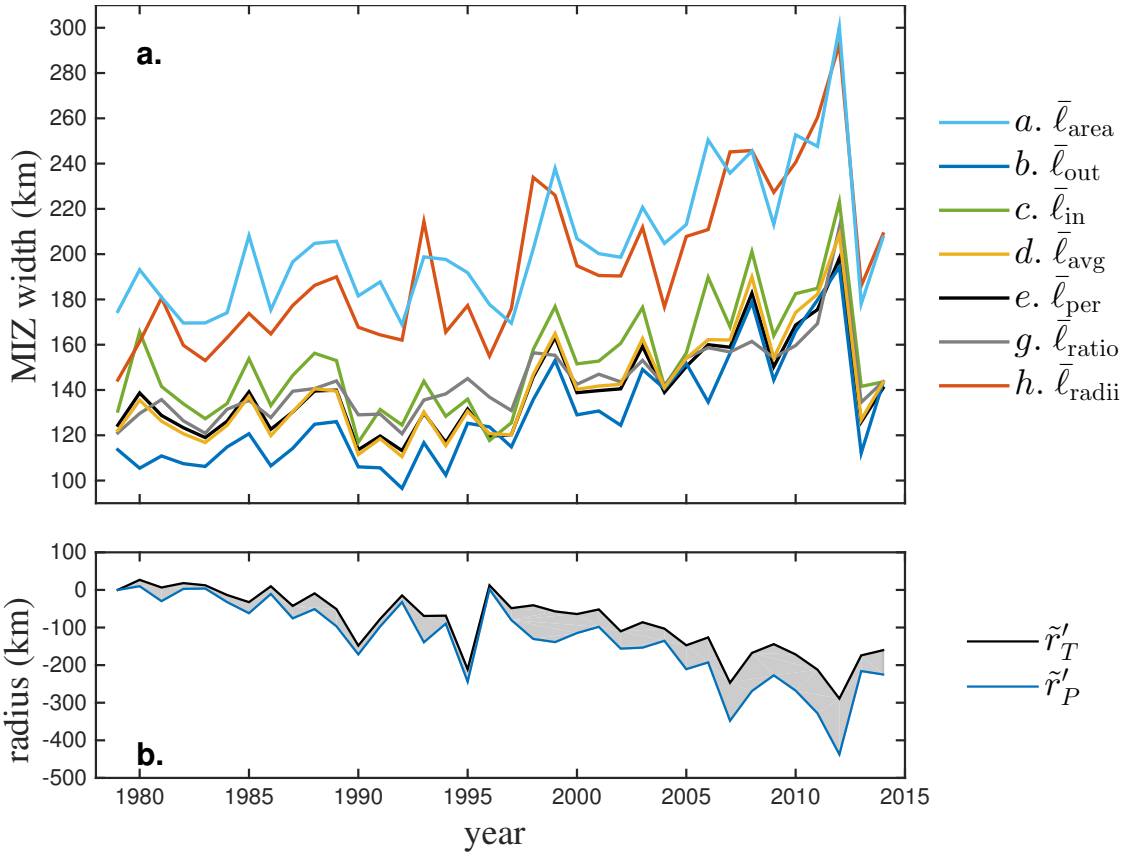

FIG. 6. (a) Average MIZ width based on analysis of satellite data. Letters in the legend refer to the formulas in Table 1. Curve for formula f is not included because of ambiguity in how its formula would be applied to satellite data (Section 4). (b) Effective radii of the total ice area ($\tilde{r}_T$) and pack ice area ($\tilde{r}_P$), shown as anomalies relative to their values in 1979.

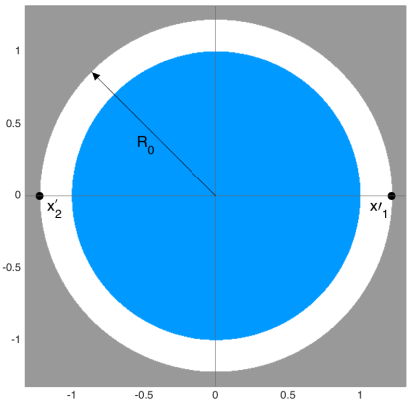

Fig. A1. Conformal mapping of the eccentric annulus from the $z-$ *plane* in Fig. 2a to the w-plane.

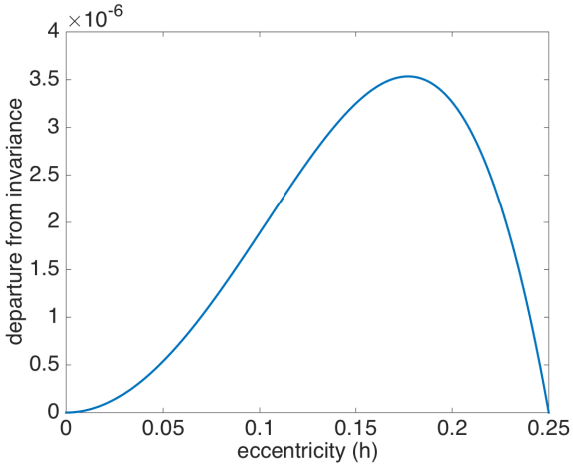

Fig. B1. Enter the caption for your figure here. Repeat as necessary for each of your figures.